

Campbell penetration depth in low carrier density superconductor YPtBi

Hyunsoo Kim^{1,2,3,4,*}, Makariy A. Tanatar^{1,2}, Halyna Hodovanets^{1,2,3,4}, Kefeng Wang,³
 Johnpierre Paglione³, and Ruslan Prozorov^{1,2,†}

¹Ames Laboratory, U.S. Department of Energy, Ames, Iowa 50011, USA

²Department of Physics and Astronomy, Iowa State University, Ames, Iowa 50011, USA

³Maryland Quantum Materials Center, Department of Physics, University of Maryland, College Park, Maryland 20742, USA

⁴Department of Physics and Astronomy, Texas Tech University, Lubbock, Texas 79410, USA

 (Received 12 April 2021; revised 21 June 2021; accepted 28 June 2021; published 16 July 2021)

Magnetic penetration depth, λ_m , was measured as a function of temperature and magnetic field in single crystals of low carrier density superconductor YPtBi by using a tunnel-diode oscillator technique. Measurements in zero DC magnetic field yield London penetration depth, $\lambda_L(T)$, but in the applied field the signal includes the Campbell penetration depth, $\lambda_C(T)$, which is the characteristic length of the attenuation of small excitation field, H_{AC} , into the Abrikosov vortex lattice due to its elasticity. Whereas the magnetic field dependent λ_C exhibit $\lambda_C \sim B^p$ with $p = 1/2$ in most of the conventional and unconventional superconductors, we found that $p \approx 0.23 \ll 1/2$ in YPtBi due to rapid suppression of the pinning strength. From the measured $\lambda_C(T, H)$, the critical current density is $j_c \approx 40$ A/cm² at 75 mK. This is orders of magnitude lower than that of conventional superconductors of comparable T_c .

DOI: [10.1103/PhysRevB.104.014510](https://doi.org/10.1103/PhysRevB.104.014510)

I. INTRODUCTION

The superconducting phase transition temperature T_c of the Bardeen-Cooper-Schrieffer (BCS) superconductors is typically of the order of $\sim 10^{-4}T_F$, where $T_F \sim 10^4\text{--}10^5$ K is the Fermi temperature [1,2]. This follows from the small value of the energy gap in the density of states, $\Delta(0) \approx 1.76k_B T_c \approx 2\hbar\omega_D \exp(-1/VN_0)$. For example, for $T_c = 10$ K, $\Delta(0) \approx 1.5$ meV $\ll E_F \sim 1\text{--}10$ eV. Here ω_D is the Debye frequency, V is the attractive pairing potential, and N_0 is the density of states at the Fermi energy E_F . N_0 has an exponential role in determining the T_c which is often estimated from the semiphenomenological McMillan equation [3,4]:

$$T_c \approx \frac{2\hbar\omega_D}{1.76k_B} \exp\left[\frac{-1.04(1+\lambda)}{\lambda - \mu^*(1+0.62\lambda)}\right], \quad (1)$$

where λ is the electron-phonon coupling parameter and μ^* is the screened Coulomb interaction constant. The weak-coupling BCS formula can be recovered by replacing $(\lambda - \mu^*)$ with the product VN_0 in the limit of small $\lambda \ll 1$. This relation was successfully applied for many intermetallic compounds with a typical carrier density $n \sim 10^{22}$ cm⁻³ [5].

However, discovery of superconductivity in materials with a poor metallic normal state with $n \sim 10^{17}\text{--}10^{19}$ cm⁻³ challenged the conventional approach. Such low n superconductors include elemental bismuth [6], SrTiO₃ [7], and half-Heusler compound RTBi (R =rare earth, T =Pd or Pt) [8–11]. The observed T_c 's (and often critical fields) in these materials are by orders of magnitude higher than the expected

T_c from the McMillan formula [12]. These low n superconductors have naturally much higher values of the ratio T_c/T_F , pushing them closer to the Bose-Einstein condensation (BEC) regime in which the spatial range of attractive interaction in the Cooper pair, the superconducting coherence length, ξ , becomes comparable to the characteristic length associated with the Fermi momentum, $\xi \sim \hbar/p_F$. In YPtBi the $k_F \approx 0.4$ nm⁻¹, whereas in SrPd₂Ge₂ with a similar T_c it is $k_F \approx 10$ nm⁻¹. There are materials believed to be in the BCS-BEC crossover regime, notably FeSe_{1-x}S_x [13].

Determination of the Cooper-pair density n_s is required to confirm the unusual low n nature of superconductivity in the material of interest. Traditionally, the normal state electronic concentration n is used to estimate n_s by using a simple relation $n_s = n/2$. While the relation usually holds in the normal metals, accurate measurements of n in the normal state with $E_F \ll 1$ eV can be challenging due to strong temperature dependence of n at low temperatures, anomalous Hall effect, and the presence of the surface states. Here we probe n_s directly in the superconducting state of YPtBi by determining the theoretical critical current density j_c , the quantity directly proportional to n_s .

The half-Heusler compound YPtBi is a topological semimetal with $n \sim 10^{18}$ cm⁻³ at low temperatures [9,14]. Its superconductivity is attracting considerable attention because T_c is about fourfold higher than that of doped SrTiO₃ with a similar $n \sim 10^{18}$ cm⁻³, and it was suggested that its superconductivity arises from the $j = 3/2$ Fermi surface [15]. The possible superconducting states include unprecedented spin-*quintet* and *septet* states [15,16]. The topological normal state is driven by strong spin-orbit coupling that inverts the s -orbital derived Γ_6 band and the p -orbital derived Γ_8 band [15]. The chemical potential lies about 35 meV below a quadratically

*hyunsoo.kim@ttu.edu

†prozorov@ameslab.gov

touching point of Γ_8 bands [9,15] due to naturally occurring crystal imperfection [17].

Recent experimental results support unconventional superconductivity in YPtBi. T_c can be enhanced by physical pressure with an initial linear rate of 0.044 K/GPa [18]. The upper critical field at zero temperature is $\mu_0 H_{c2}(0) = 1.5$ T [9], which is higher than the Pauli limiting field 1.4 T [9] for a weak-coupling spin-1/2 singlet superconductor. The temperature dependence of $H_{c2}(T)$ is practically linear over almost an entire superconducting temperature range; quite different from conventional parabolic behavior [9]. A muon spin rotation study determined $\lambda_L(0) = 1.6$ μm [19], which is an order of magnitude greater than that of the strong type-II superconductor CeCoIn₅ where $\lambda(0) \approx 0.26$ μm [20]. Coherence length at zero temperature is $\xi(0) = \sqrt{\phi_0/2\pi H_{c2}(0)} \approx 15$ nm. The Ginzburg-Landau parameter is $\kappa = \lambda_L(0)/\xi(0) \approx 10^2 \gg 1/\sqrt{2}$, placing it in the strong type-II regime of superconductivity.

In the mixed state of a type-II superconductor, the small-amplitude AC magnetic penetration depth is governed by the elastic properties of the Abrikosov vortex lattice in the linear response regime. This means that the amplitude of the AC field excitation, H_{AC} , is not large enough to displace the vortex out of the pinning potential well, and it only perturbs the vortex position within the validity of Hooke's law. In this case, the penetration depth is described by the Campbell penetration depth λ_C that determines the attenuation range of the AC perturbation from the sample surface to the interior, $B_{AC}(x) \propto \mu H_{AC} e^{-x/\lambda_C}$ in a semi-infinite superconductor [21–27]. Here μ is magnetic permeability, and x is the distance from the surface. Since λ_C is not commonly measured due to amplitude/sensitivity limitations of the conventional AC techniques, we provide a simple derivation of λ_C in the Appendix for completeness. The important advantage of employing λ_C is that it gives access to the shielding current density via a relation $\lambda_C^2 = H_0 r_p / j_c$. Here r_p is the radius of the pinning potential, and H_0 is the applied external DC magnetic field (see the Appendix for details). Importantly, the critical current density is estimated at the frequency of the measurement, and the rf regime gives access to almost unrelaxed values. The initial vortex relaxation is exponential, and hence the conventional techniques estimate relaxed values far from the true j_c [28–30].

While analysis of the relaxed shielding current is complicated because of inclusion of the magnetic relaxation parameters, the unrelaxed critical current, $j_c = H_0 r_p / \lambda_C^2$, offers direct access to the superfluid density $n_s \propto j_c$ [2,31,32]. In this work, we use a tunnel diode oscillator (TDO) technique to measure $\lambda_C(T, H)$ and determine $j_c(T, H)$ in YPtBi. The determined j_c is orders of magnitude smaller than that of well-known superconductors with the typical carrier density, and its rapid suppression by the magnetic field provides valuable insight into the fascinating nature of superconductivity at the low carrier density regime exemplified by YPtBi.

II. EXPERIMENT

YPtBi single crystals were grown out of molten Bi with starting composition Y:Pt:Bi = 1:1:20 (atomic ratio) [9,15,33,34]. The starting materials Y ingot (99.5%), Pt

powder (99.95%), and Bi chunk (99.999%) were put into an alumina crucible, and the crucible was sealed inside an evacuated quartz ampule. The ampule was heated slowly to 1150 °C, kept for 10 h, and then cooled down to 500 °C at a 3 °C/h rate, where the excess of molten Bi was decanted by centrifugation.

The variation of the rf magnetic penetration depth $\Delta\lambda_m$ was measured in a dilution refrigerator by using a TDO technique [35] (for review, see Refs. [36,37]). The sample with dimensions $(0.29 \times 0.69 \times 0.24)$ mm³ positioned with the shortest direction along H_{AC} was mounted on a sapphire rod and inserted into a 2-mm inner diameter copper coil that (when empty) produces rf excitation field with amplitude $H_{AC} \approx 20$ mOe and frequency of $f_0 \approx 22$ MHz. The shift of the resonant frequency (in cgs units), $\Delta f(T) = -G4\pi\chi(T)$, where $\chi(T)$ is the differential magnetic susceptibility, $G \approx f_0 V_s / 2V_c(1-N)$ is a constant, N is the effective demagnetization factor, V_s is the sample volume, and V_c is the coil volume [36]. The constant G was determined from the full frequency change by physically pulling the sample out of the coil. With the characteristic sample size, R , $4\pi\chi = (\lambda_m/R) \tanh(R/\lambda_m) - 1$, from which $\Delta\lambda_m$ can be obtained [36].

III. RESULTS

Figure 1(a) shows temperature variation of the rf magnetic penetration depth $\lambda_m(T)$ in a single crystal of YPtBi in various applied DC magnetic fields H_{DC} from 0 to 30 kOe (bottom to top). For $H_{DC} = 0$, measured $\Delta\lambda_m(T)$ is the zero field limiting London penetration depth $\Delta\lambda_L(T)$ which exhibits a sharp superconducting phase transition at $T \approx 0.8$ K. We found $\Delta\lambda_L(T) = AT^\alpha$ where $A = 1.98$ $\mu\text{m}/\text{K}^\alpha$ and $\alpha = 1.2$ [15]. The observed exponent α is consistent with the presence of line nodes in the superconducting gap and moderate impurity scattering. The large prefactor, $A \propto \lambda_L(0)/\Delta(0)$ is compatible with a low carrier density superconductor within London theory $\lambda_L(0) = (mc^2/4\pi ne^2)^{1/2}$. For comparison, $A = 4\text{--}15$ $\text{\AA}/\text{K}$ is observed in *d*-wave line-nodal high-temperature cuprate superconductors [38] and 190–370 $\text{\AA}/\text{K}$ in CeCoIn₅ [20,39,40].

Furthermore, YPtBi exhibits very pronounced field dependence of λ_m . It is notable even at the lowest $H_{DC} = 100$ Oe which is $0.007H_{c2}(0)$. Here we use $H_{c2}(0) = 15$ kOe taken from Ref. [9]. By measuring $\lambda_m(H, T)$ as a function of temperature in different applied fields we constructed the magnetic field temperature H - T phase diagram of YPtBi. Due to the broadness of the superconducting transition, we used three different criteria for the determination of T_c , as illustrated in the inset of Fig. 1(b). T_1 was determined at the sharp maximum of $d\lambda_m/dT$ (black squares). T_2 was determined at the intersection of the lines through the data in the superconducting state and the normal states (blue circles). T_3 was determined at the onset of $\Delta\lambda_m(T)$ deviation from the normal state behavior (red up-triangles). The phase diagram from rf magnetic penetration depth data is shown in the main panel of Fig. 1(b). For reference, we show the diagram as determined from resistivity measurements by Butch *et al.* [9], using zero resistivity (black solid line), crossing point of linear extrapolations (blue dashes), and onset of deviation (red dash-dot)

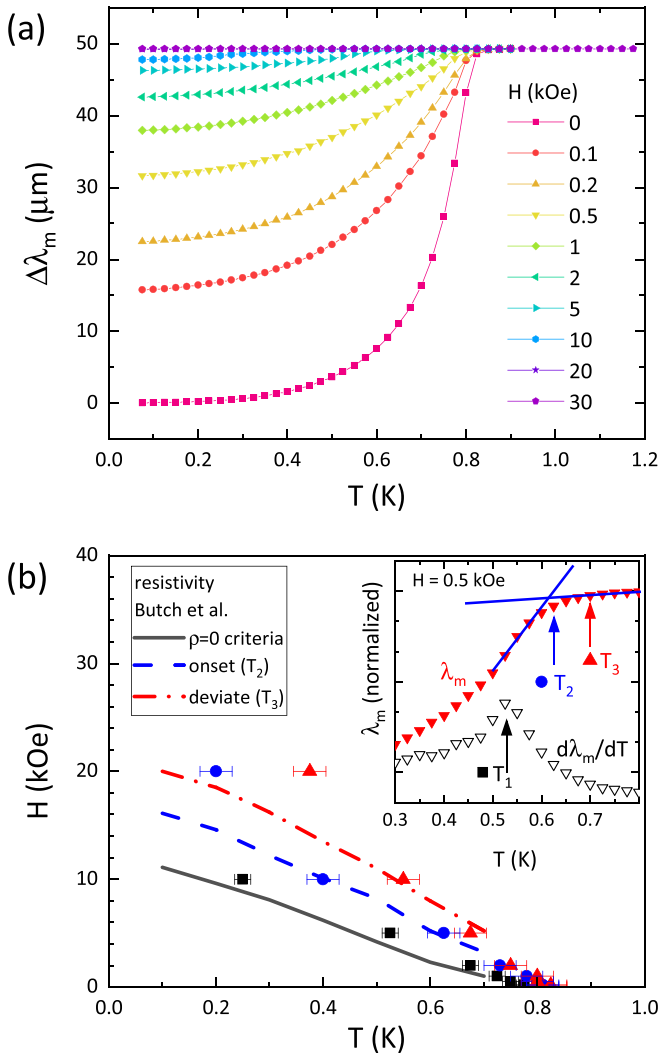


FIG. 1. (a) Temperature variation of the radio-frequency magnetic penetration depth, $\Delta\lambda_m(T)$, in various applied DC magnetic fields H_{DC} . (b) The H - T phase diagram constructed from $\Delta\lambda_m(T, H)$ using characteristic temperatures, T_1 (maximum of $d\lambda_m/dT$, black squares), T_2 (crossing point of linear extrapolations, blue circles), and T_3 (onset of deviation, red up-triangles) as shown in the inset. The lines in the main panel of (b) show for reference the H - T phase diagram as determined from the field-dependent electrical resistivity by zero resistivity (black), crossing point of linear extrapolations (blue dashes), and onset of deviation (red dash-dot) criteria [9].

criteria. The phase diagram as determined from maximum of $d\lambda_m/dT$ line is closely following the phase diagram as determined from resistivity measurements using $\rho = 0$ criteria [9]. However, we detected an apparent diamagnetic response in YPtBi at notably higher fields than in resistivity measurements, suggesting persistence of superconductivity in some nonbulk form [41]. A discrepancy between H_{c2} as determined from bulk thermal conductivity and nonbulk resistivity measurements is a known problem [42] and it is usually assigned to the superconducting layer surviving at the surface. Perhaps it is related to the third critical field in superconductors predicted theoretically by Saint-James and Gennes [43] when a thin superconducting layer is formed on the flat surface

parallel to the field. Recently, a surface-sensitive tunneling experiment on YPtBi detected energy gap spectra at higher temperatures than $T_c \approx 0.8$ K [44]. A similar signature of the superconducting phase was reported in another half-Heusler compound LuPtBi, which was attributed to the presence of Van Hove singularity near E_F [45] and surface pairing states [46]. The shape of tunneling spectra in the superconducting state is inconsistent with an isotropic s -wave gap in both YPtBi and LuPtBi [44,45].

We focus now on the variation of λ_m with finite H_{DC} in the mixed state. The measured magnetic penetration depth satisfies the relation $\lambda_m^2 = \lambda_L^2 + \lambda_C^2$ in the approximation of a linear elastic response of a vortex lattice to a small amplitude AC perturbation H_{AC} [21–23]. The TDO technique is a perfect probe for this measurement because of small frequency, $f_0 = 22$ MHz, and small amplitude of the perturbation, $H_{AC} = 20$ mOe. Since $\lambda_L(T) = \lambda_L(0) + \Delta\lambda_L(T)$ where $\lambda(0) = 1.6 \mu\text{m}$ [19], we can readily calculate $\lambda_C(T)$ in various H_{DC} . However, we took a conservative approach, assuming that this approximation is valid only at temperatures below $0.5T_1$ because $\lambda_m(T)$ becomes comparable to the size of the sample as temperature increases towards T_c . The calculated $\lambda_C = \sqrt{\lambda_m^2 - \lambda_L^2}$ at various H_{DC} is shown in Fig. 2(a). In all measured H_{DC} , $\lambda_C(T)$ shows monotonic increase with temperature as the superconductor allows more penetration of the rf field with increasing temperature.

Figure 2(b) shows the field-dependent $\lambda_C^2(H)$ at several temperatures. When critical current density does not vary much with field, we expect $\lambda_C^2(H) \sim H$ and it has been observed in most cases [41,47,48]. However, YPtBi exhibits significantly more curved $\lambda_C^2(H)$, indicating nearly logarithmic behavior at low fields. This rapid rise of $\lambda_m(H)$ at low fields is unusual but may be explained considering very large values of λ_m leading to strong intervortex interaction due to significant overlap already in low fields.

In Fig. 3, we compare this anomalous $\lambda_C(H)$ in YPtBi with SrPd₂Ge₂ which has a normal carrier density and exhibits H -linear behavior of $\lambda_C^2(H)$. The observed power-law behavior of the Campbell penetration depth is highly unusual, and it is one of the most significant observations in this work. Typically, λ_C varies as $H^{1/2}$, but we found that it varies as $H^{1/4}$ in YPtBi. The power-law behavior can be explained if the Labusch parameter is field dependent and varies as $H^{1/2}$, which is consistent with increasing the effective size of the pinning potential. Alternative possibilities include the anharmonic pinning potential or the breakdown of the conventional picture of Campbell penetration depth.

As noted above from the known $\lambda_C(T, H)$, one can evaluate critical current density j_c via $j_c = H_{DC}r_p/\lambda_C^2$ (see the Appendix for details) where r_p is a characteristic radius of the pinning potential, usually taken equal to the coherence length, $r_p(T) = \xi(T)$ [21,22,41,47,48]. Figure 4 shows the calculated $j_c(T)$ in YPtBi, obtained from $\lambda_C(T)$ measurements taken in minimum applied $H_{DC} = 100$ Oe. We compare $j_c(T)$ in YPtBi to the j_c 's determined in similar Campbell penetration depth measurements in some representative superconductors, LiFeAs [49] and SrPd₂Ge₂ [41]. The former is known as a two-band superconductor with full gaps [50], and the latter is a single-gap BCS superconductor [41]. The compared $j_c(T, H)$ in these superconductors were obtained by using the same

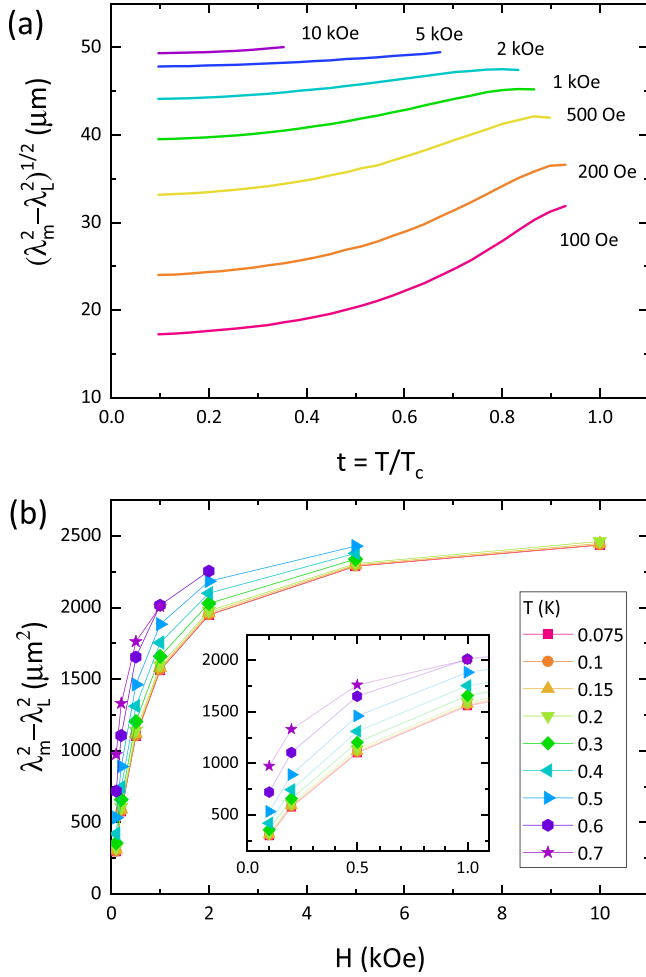


FIG. 2. (a) Temperature variation of the Campbell length $\lambda_C(T) = \sqrt{\lambda_m^2(T) - \lambda_L^2(T)}$ in DC magnetic fields H_{DC} as indicated in the panel. (b) Isotherms of field variation of $\lambda_C^2(H)$ in YPtBi. Inset shows zoom of the low-field regime.

TDO technique. In particular, we used the same TDO setup for YPtBi and SrPd₂Ge₂.

In YPtBi, the highest $j_c(T) \approx 40$ A/cm² is observed at $T \approx 75$ mK, and $j_c(T)$ monotonically decreases with temperature. In LiFeAs, $j_c \approx 1 \times 10^6$ A/cm² at the lowest temperature, and it monotonically decreases by two orders of magnitude upon warming. In SrPd₂Ge₂, $j_c \approx 8.3 \times 10^4$ A/cm² at the lowest temperature with $H_{\text{DC}} = 200$ Oe. However, its temperature variation is nonmonotonic and exhibits a maximum at an intermediate temperature, which was attributed to a matching effect between temperature-dependent coherence length and relevant pinning length scale [41]. At a higher $H_{\text{DC}} = 4$ kOe, $j_c(T)$ recovers a monotonic decrease with increasing temperature. Even when $T_{\text{sc}}(H)$ of SrPd₂Ge₂ was reduced to 0.86 K in $H_{\text{DC}} = 4$ kOe which is close to T_{sc} of YPtBi with 100 Oe, j_c is still two orders of magnitude greater, and the difference gets even bigger at base temperature. It is also instructive to calculate the depairing current density at which Cooper pairs break apart reaching critical velocity, $4\pi c^{-1} j = \phi_0 / (3\sqrt{3}\lambda_L^2 \xi) \approx 1 \times 10^7$ A/cm², which is much larger than j_c due to pinning, but two orders

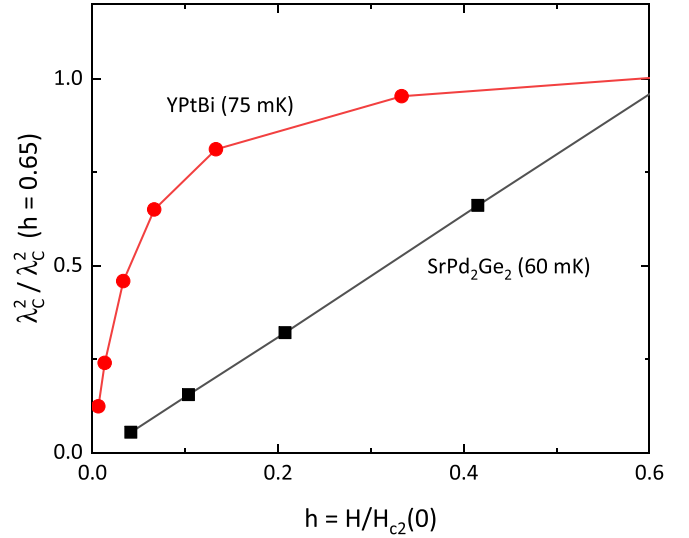


FIG. 3. Field-dependent Campbell penetration depth $\lambda_C^2(H)$ of YPtBi (red line with solid circles) shown in comparison with conventional metal/superconductor with similar T_c , SrPd₂Ge₂. The data are normalized to the values determined at $0.65H_{c2}(0)$ for clarity.

of magnitude less than in “typical” normal carrier density superconductors [28,30].

In Table I, we compare normal state Hall constants R_H reported for YPtBi [9] and SrPd₂Ge₂ [51]. In both compounds the Hall resistivity $\rho_{xy}(H)$ is field linear, which enables R_H definition from the slope of the curve and sample geometry. The reported R_H values are -1.6×10^{-4} cm³/C [51] and $+2.4$ cm³/C [9] for SrPd₂Ge₂ and YPtBi, respectively. In the single-band Drude model, the carrier density satisfies a simple relation, $R_H = 1/ne$ where e is the electron charge. The

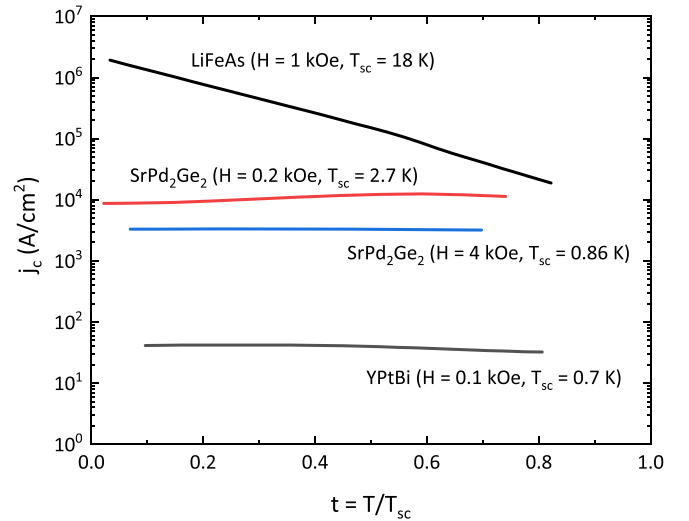


FIG. 4. Temperature variation of the theoretical critical current density $j_c(T)$ in a selection of superconductors. We show the data in YPtBi in comparison with iron-based stoichiometric clean LiFeAs, and the low-temperature conventional superconductor SrPd₂Ge₂ measured in two different magnetic fields. T_{sc} stands for the superconducting transition at a given magnetic field. For YPtBi, $T_{\text{sc}} = T_1$ (see Fig. 1).

TABLE I. Hall constant R_H , n , and j_c in YPtBi and SrPd₂Ge₂.

	R_H (cm ³ /C)	n (cm ⁻³)	j_c (A/cm ²)
YPtBi	+2.4 [9]	2.6×10^{18}	40 ^a
SrPd ₂ Ge ₂	-1.6×10^{-4} [51]	3.9×10^{22}	8300 ^b

^aDetermined at 75 mK ($0.096T_c$) and 100 Oe [$0.007H_{c2}(0)$].

^bDetermined at 60 mK ($0.022T_c$) and 200 Oe [$0.042H_{c2}(0)$].

calculated carrier densities are electronlike $n_e = 3.9 \times 10^{22}$ cm⁻³ for SrPd₂Ge₂ and holelike $n_h = 2.6 \times 10^{18}$ cm⁻³ for YPtBi. For reference we also present j_c in both SrPd₂Ge₂ and YPtBi in Table I.

IV. DISCUSSION

The carrier density n is responsible for the observed theoretical current density because $j_c \propto n_s v_s$ where v_s is the velocity of the supercurrent [2,31,32]. Provided $n_s \approx n/2$, j_c in YPtBi is two orders of magnitude smaller than that in SrPd₂Ge₂, while the normal state n in YPtBi is smaller by four orders of magnitude. Consequently, v_s in YPtBi is two orders of magnitude greater than that in SrPd₂Ge₂.

In Ginzburg-Landau theory, j_c is associated with the depairing velocity $v_s = \Delta(0)/\hbar k_F$, and since $\Delta(0)$ values in both superconductors are of the same order, the different v_s is accounted by different k_F values in these two compounds. In SrPd₂Ge₂, $k_F \approx 10$ nm⁻¹ in free electron approximation, i.e., $k_F = (3\pi^2 n)^{1/3}$ with $n = 2.6 \times 10^{22}$ cm⁻³ which is about two orders of magnitude greater than that in YPtBi, $k_F = 0.37$ nm⁻¹ [15]. We note that the expression for the depairing velocity used above was originally derived in the context of the BCS theory, and it uses the concept of diminishing superconducting energy gap due to additional kinetic energy. However, this relation could be used in any type of superconductors although the magnitude of the depairing velocity cannot be determined accurately. Hence, this expression should be used with caution. We employ this expression to reconcile the orders of difference in the magnitude of the critical current density between SrPd₂Ge₂ and YPtBi, and it provides a reasonable explanation about it.

There has been much effort to elucidate the unconventional superconductivity in the low carrier density superconductors including YPtBi and SrTiO₃. Recently, the unexpectedly high T_c in YPtBi was explained by the electron-phonon pairing mechanism with polar optical phonon mode within the $j = 3/2$ Luttinger-Kohn four-band model [52]. In the similar low carrier density superconductors, the plasmonic [53] and nonadiabatic [54] superconducting mechanisms were proposed in SrTiO₃.

The structure of the superconducting energy gap and the symmetry of pairing interaction are prerequisites for understanding the superconducting mechanism, but low T_c in the low n superconductors makes the experimental investigation difficult. The half-Heusler compounds $RTBi$ ($R=Y,La,Lu$; $T=Pt,Pd$) exhibit relatively high superconducting transition temperatures $T_c \sim 1$ K [9–11], and a nodal superconducting gap was observed in YPtBi [15]. Subsequently, various exotic pairing symmetries were proposed including nematic d -wave [55,56] and $j = 3/2$ high-spin superconductivity

[15–17,46,57,58]. In general, the high-spin superconductivity exhibits topological gap structures with the possibility of harboring the Majorana surface fluid [46,59], which makes the low carrier density superconductor $RTBi$ a promising platform for the fault-tolerant quantum devices.

V. SUMMARY

We measured rf superconducting magnetic penetration depth in single-crystal YPtBi. The London penetration depth is consistent with the nodal superconductivity in YPtBi. In the finite DC magnetic fields, the measured Campbell penetration depth exhibits unusual subquadratic power-law behavior in the low-field range. From the variation of the Campbell penetration depth, we estimated the theoretical critical current density which is orders of magnitude smaller than that of the superconductors with a typical carrier density. Therefore, we confirmed the low carrier density nature of superconductivity in YPtBi.

ACKNOWLEDGMENTS

We would like to thank V. G. Kogan for the useful discussion. Work in Ames was supported by the US Department of Energy (DOE), Office of Science, Basic Energy Sciences, Materials Science and Engineering Division. Ames Laboratory is operated for the US DOE by Iowa State University under Contract No. DE-AC02-07CH11358. Research done at the University of Maryland was supported by the US Department of Energy (DOE) Award No. DE-SC-0019154 (experimental investigations), and the Gordon and Betty Moore Foundation EPIQS Initiative through Grant No. GBMF9071 (materials synthesis).

APPENDIX: ILLUSTRATION OF THE CONCEPT OF CAMPBELL LENGTH

Here we provide simple arguments behind the concept of pinning and Campbell penetration depth. This physics has been discussed multiple times in the past 80 years and is textbook material. However, we felt that it is instructive to write down the derivation with units and show step by step the flow. There is still a significant degree of confusion dealing with currents, fields, and flux in cgs and SI. There is also some confusion about the Campbell penetration depth written for a single vortex featuring single flux quanta ϕ_0 vs what should be with the magnetic induction, B , recognizing that this is a collective effect. This is because the critical current density is introduced via the single vortex pinning. Unfortunately, the original derivation by Campbell [21,22] is too short and too schematic to our taste and we wanted to explain everything step by step.

1. Single vortex pinning

Figure 5 shows the schematics of the vortices and pinning potential model. The vortices move along the horizontal x axis, the electrical current flows into or out of the page along the y axis, and the external magnetic field is applied along the positive vertical direction of the z axis. The displacement $u(x)$ is the deviation of a vortex from the center of its potential well.

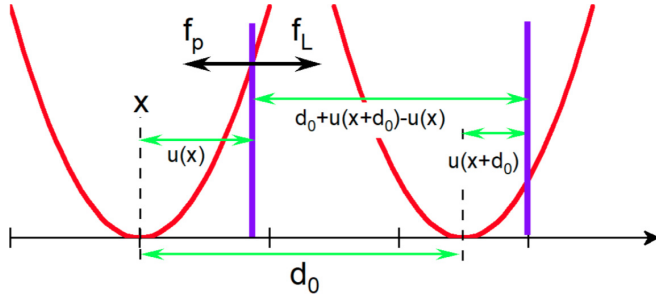


FIG. 5. Schematic for movement of vortices in the pinning potential. The violet vertical bars represent vortices, and the red parabolas are the pinning potential, $U(u)$. The vortices move along the horizontal line (x axis), the electrical current flows into or out of the page (y axis), and the external magnetic field is applied along the positive vertical axis (z axis). The displacement u stands for the horizontal position of each vortex from the equilibrium point.

In equilibrium, $u(x) = 0$ for all vortices and their distribution is constant.

Assuming a vortex along the positive z axis in a pinning potential $U(u)$ (real units energy distance), then for a single vortex, the Lorentz force *per unit length* is

$$\mathbf{f}_L \left[\frac{\text{N}}{\text{m}} \right] = \mathbf{j} \left[\frac{\text{A}}{\text{m}^2} \right] \times \hat{\mathbf{z}} \phi_0 [\text{T m}^2]. \quad (\text{A1})$$

Here, $\phi_0 = 2.068 \times 10^{-15} \text{ Wb} = \text{T m}^2$. (Note, we use SI units throughout the Appendix.)

The electrical current density \mathbf{j} along the positive y direction would push the vortices to the positive x direction with the magnitude, $f_L = j\phi_0$. It is usually assumed that the pinning potential is given by

$$U(u) = \frac{1}{2} \alpha u^2 \left[\frac{\text{J}}{\text{m}} \right], \quad (\text{A2})$$

where α is the so-called Labusch parameter:

$$\alpha = \frac{d^2 U(u)}{du^2} \left[\frac{\text{J}}{\text{m}^3} \right]. \quad (\text{A3})$$

The pinning force due to $U(u)$ is defined by

$$f_p = -\frac{dU(u)}{du} = -\alpha u. \quad (\text{A4})$$

In the presence of the electrical current, the two forces, \mathbf{f}_L and \mathbf{f}_p , will act on a vortex in the opposite directions, i.e., $f_L + f_p = 0$. In this case, the critical current density, j_c , is reached when the magnitudes of two forces become equal at a distance $u = r_p$ that is called the “radius of the pinning potential.” In equilibrium, $j_c \phi_0 = \alpha r_p$, and therefore j_c can be expressed as

$$j_c = \frac{\alpha r_p}{\phi_0} \left[\frac{\text{A}}{\text{m}^2} \right]. \quad (\text{A5})$$

The major contribution to pinning comes from the gain of free energy in the normal core volume of a vortex and, therefore, r_p is usually assumed to be equal to the superconducting coherence length ξ . Of course, the pinning theory is much more complex, and the readers are referred to the excellent review articles, Refs. [23,28].

2. The Campbell penetration depth

The Campbell length λ_C is defined for a large number of vortices since this is a wavelike perturbation in the vortex lattice treated as an elastic medium [23,28]. In other words, λ_C determines how far a small-amplitude AC perturbation on the superconductor edge propagates into the vortex lattice. [21]. Let us assume a uniform distribution of vortices [e.g., after field cooling (FC)] and hence a uniform magnetic induction B_0 . We apply a small AC field on the sample edge, i.e., $B = B_0 + B_{AC}$, where $B_{AC} \ll B_0$. In equilibrium, the vortices are equally spaced by the distance d_0 found from the condition that each vortex carries a single flux quantum, ϕ_0 :

$$d_0 = \sqrt{\frac{\phi_0}{B_0}} = \frac{45.473}{\sqrt{B[\text{T}]}} [\text{nm}]. \quad (\text{A6})$$

Here we assumed a square vortex lattice instead of triangular for simplicity, which does not alter the results.

Consider a one-dimensional problem (semi-infinite superconductor positioned at $x \geq 0$) with a magnetic field applied along the positive z axis and electric current flowing along the positive y axis. At a distance, x , from the edge, a row of vortices uniformly spaced along the y axis is displaced by $u(x)$ from their equilibrium positions. The next row of vortices is displaced by the distance $d_0 + u(x + d_0) - u(x)$ counted from the first row of vortices (see Fig. 5). Therefore, the distance between the vortices, $d(x)$, satisfies

$$d(x) = d_0 \left[1 + \frac{u(x + d_0) - u(x)}{d_0} \right] \approx d_0 \left(1 + \frac{du}{dx} \right) \quad (\text{A7})$$

because d_0 is the smallest physical distance in the problem. Therefore, the magnetic induction B at the location x is given by

$$B(x) = \frac{\phi_0}{d d_0} = \frac{\phi_0}{d_0^2 \left(1 + \frac{du}{dx} \right)} = B_0 \left(1 - \frac{du}{dx} \right), \quad (\text{A8})$$

where we assume that $\frac{du}{dx} \ll 1$, which can be easily checked with the final solution for $u(x)$. Note that if all vortices were displaced uniformly, $u = \text{const}$, then $B(x)$ remains unchanged.

This perturbation of $B(x)$ corresponds to the current density from the Maxwell equation, $\mu_0 \mathbf{J} = \nabla \times \mathbf{B}$. Assuming $\mathbf{B} = B(x) \hat{\mathbf{z}}$,

$$\mu_0 J_y = -\frac{\partial B(x)}{\partial x} = B_0 \frac{d^2 u}{dx^2}. \quad (\text{A9})$$

The Lorentz force on vortices per unit volume is

$$F_L = J B_0 = \frac{B_0^2}{\mu_0} \frac{d^2 u}{dx^2}, \quad (\text{A10})$$

which must be balanced by the pinning force. From the previous (single vortex) section, each vortex experiences pinning force per unit length, $f_p = -\alpha u$, and there are approximately $N = B_0/\phi_0$ vortices per unit area. The total pinning force *per unit volume*, F_p , can be written in the form

$$F_p = N f_p = -\frac{\alpha B_0}{\phi_0} u. \quad (\text{A11})$$

The two forces, F_L and F_p , balance each other in the steady state, and the characteristic penetration depth is determined from the following relation:

$$F_L + F_p = \frac{B_0^2}{\mu_0} \frac{d^2 u}{dx^2} - \frac{\alpha B_0}{\phi_0} u = 0 \quad (\text{A12})$$

or

$$\lambda_C^2 \frac{d^2 u}{dx^2} = u. \quad (\text{A13})$$

Here we introduced the Campbell length:

$$\lambda_C^2 = \frac{\phi_0 B_0}{\mu_0 \alpha} \left[\frac{T^2 m^2}{\frac{H}{m} \frac{J}{m^3}} = m^2 \right]. \quad (\text{A14})$$

Note that the radius of the pinning potential, r_p , does not explicitly enter here. This is true only for parabolic pinning potential within the validity of Hooke's law for vortex displacement. The nonparabolic potentials have also been considered and lead to a variety of interesting effects [24,26,27,60].

The Labusch constant α can be evaluated from the measured λ_C by using (A14). The solution of Eq. (A13) for u is

$$u(x) = u_0 e^{-x/\lambda_C}. \quad (\text{A15})$$

Therefore the magnetic induction can be found by using (A8) as follows:

$$B(x) = B_0 \left(1 - \frac{du}{dx} \right) = B_0 \left(1 + \frac{u_0}{\lambda_C} e^{-x/\lambda_C} \right). \quad (\text{A16})$$

At the boundary, $x = 0$, and $B = B_0 + B_{AC}$ where

$$B_{AC} = B_0 \frac{u_0}{\lambda_C}, \quad u_0 = \lambda_C \frac{B_{AC}}{B_0}.$$

The displacement $u(x)$ in terms of B_{AC} and B_0 can be written in the form

$$u(x) = \lambda_C \frac{B_{AC}}{B_0} e^{-x/\lambda_C} \quad (\text{A17})$$

and we can express $B(x)$ as

$$B(x) = B_0 \left(1 + \lambda_C \frac{B_{AC}}{B_0} \frac{u_0}{\lambda_C} e^{-x/\lambda_C} \right) = B_0 + B_{AC} e^{-x/\lambda_C}, \quad (\text{A18})$$

which is expected from the boundary conditions.

Finally, we derive a practical expression for J_c in terms of λ_C that can be experimentally determined. Using (A18),

$$\lambda_C^2 = \frac{\phi_0 B_0}{\mu_0 \alpha} = \frac{\phi_0 H}{\alpha},$$

$$\frac{\phi_0}{\alpha} = \lambda_C^2 \frac{\mu_0}{B_0}.$$

Thus, J_c is related to λ_C as follows:

$$J_c = \frac{\alpha r_p}{\phi_0} = \frac{B_0 r_p}{\mu_0 \lambda_C^2} = \frac{H_0 r_p}{\lambda_C^2}. \quad (\text{A19})$$

We use the relation (A19) to calculate the critical current density from the measured Campbell penetration depth in the main text.

-
- [1] J. Bardeen, L. N. Cooper, and J. R. Schrieffer, *Phys. Rev.* **108**, 1175 (1957).
- [2] M. Tinkham, *Introduction to Superconductivity*, 2nd ed. (Dover, New York, 2004).
- [3] W. L. McMillan, *Phys. Rev.* **167**, 331 (1968).
- [4] P. B. Allen and R. C. Dynes, *Phys. Rev. B* **12**, 905 (1975).
- [5] R. Dynes, *Solid State Commun.* **10**, 615 (1972).
- [6] O. Prakash, A. Kumar, A. Thamizhavel, and S. Ramakrishnan, *Science* **355**, 52 (2017).
- [7] X. Lin, Z. Zhu, B. Fauqué, and K. Behnia, *Phys. Rev. X* **3**, 021002 (2013).
- [8] G. Goll, M. Marz, A. Hamann, T. Tomanic, K. Grube, T. Yoshino, and T. Takabatake, *Phys. B (Amsterdam, Neth.)* **403**, 1065 (2008).
- [9] N. P. Butch, P. Syers, K. Kirshenbaum, A. P. Hope, and J. Paglione, *Phys. Rev. B* **84**, 220504(R) (2011).
- [10] F. F. Tafti, T. Fujii, A. Juneau-Fecteau, S. René de Cotret, N. Doiron-Leyraud, A. Asamitsu, and L. Taillefer, *Phys. Rev. B* **87**, 184504 (2013).
- [11] Y. Nakajima, R. Hu, K. Kirshenbaum, A. Hughes, P. Syers, X. Wang, K. Wang, R. Wang, S. R. Saha, D. Pratt, J. W. Lynn, and J. Paglione, *Sci. Adv.* **1**, e1500242 (2015).
- [12] M. Meinert, *Phys. Rev. Lett.* **116**, 137001 (2016).
- [13] S. Kasahara, T. Watashige, T. Hanaguri, Y. Kohsaka, T. Yamashita, Y. Shimoyama, Y. Mizukami, R. Endo, H. Ikeda, K. Aoyama, T. Terashima, S. Uji, T. Wolf, H. von Löhneysen, T. Shibauchi, and Y. Matsuda, *Proc. Natl. Acad. Sci. USA* **111**, 16309 (2014).
- [14] H. Lin, L. A. Wray, Y. Xia, S. Xu, S. Jia, R. J. Cava, A. Bansil, and M. Z. Hasan, *Nat. Mater.* **9**, 546 (2010).
- [15] H. Kim, K. Wang, Y. Nakajima, R. Hu, S. Ziemak, P. Syers, L. Wang, H. Hodovanets, J. D. Denlinger, P. M. R. Brydon, D. F. Agterberg, M. A. Tanatar, R. Prozorov, and J. Paglione, *Sci. Adv.* **4**, eaao4513 (2018).
- [16] P. M. R. Brydon, L. Wang, M. Weinert, and D. F. Agterberg, *Phys. Rev. Lett.* **116**, 177001 (2016).
- [17] Y. G. Yu, X. Zhang, and A. Zunger, *Phys. Rev. B* **95**, 085201 (2017).
- [18] T. V. Bay, T. Naka, Y. K. Huang, and A. de Visser, *Phys. Rev. B* **86**, 064515 (2012).
- [19] T. Bay, M. Jackson, C. Paulsen, C. Baines, A. Amato, T. Orvis, M. Aronson, Y. Huang, and A. de Visser, *Solid State Commun.* **183**, 13 (2014).
- [20] E. E. M. Chia, D. J. Van Harlingen, M. B. Salamon, B. D. Yanoff, I. Bonalde, and J. L. Sarrao, *Phys. Rev. B* **67**, 014527 (2003).
- [21] A. M. Campbell, *J. Phys. C* **2**, 1492 (1969).
- [22] A. M. Campbell, *J. Phys. C* **4**, 3186 (1971).
- [23] E. H. Brandt, *Rep. Prog. Phys.* **58**, 1465 (1995).
- [24] R. Prozorov, R. W. Giannetta, N. Kameda, T. Tamegai, J. A. Schlueter, and P. Fournier, *Phys. Rev. B* **67**, 184501 (2003).

- [25] R. Willa, V. B. Geshkenbein, and G. Blatter, *Phys. Rev. B* **92**, 134501 (2015).
- [26] R. Willa, V. B. Geshkenbein, R. Prozorov, and G. Blatter, *Phys. Rev. Lett.* **115**, 207001 (2015).
- [27] R. Willa, V. B. Geshkenbein, and G. Blatter, *Phys. Rev. B* **93**, 064515 (2016).
- [28] G. Blatter, M. V. Feigel'man, V. B. Geshkenbein, A. I. Larkin, and V. M. Vinokur, *Rev. Mod. Phys.* **66**, 1125 (1994).
- [29] L. Burlachkov, D. Giller, and R. Prozorov, *Phys. Rev. B* **58**, 15067 (1998).
- [30] T. Kubo, *Phys. Rev. Res.* **2**, 013302 (2020).
- [31] J. Bardeen, *Phys. Rev. Lett.* **1**, 399 (1958).
- [32] L. P. Gor'kov, *Zh. Eksp. Theor. Phys.* **36**, 1918 (1959) [*Sov. Phys. JETP* **9**, 1364 (1959)].
- [33] P. C. Canfield, J. D. Thompson, W. P. Beyermann, A. Lacerda, M. F. Hundley, E. Peterson, Z. Fisk, and H. R. Ott, *J. Appl. Phys.* **70**, 5800 (1991).
- [34] P. C. Canfield and Z. Fisk, *Philos. Mag.* **B 65**, 1117 (1992).
- [35] H. Kim, M. A. Tanatar, and R. Prozorov, *Rev. Sci. Instrum.* **89**, 094704 (2018).
- [36] R. Prozorov and R. W. Giannetta, *Supercond. Sci. Technol.* **19**, R41 (2006).
- [37] R. Prozorov and V. G. Kogan, *Rep. Prog. Phys.* **74**, 124505 (2011).
- [38] R. Prozorov, R. W. Giannetta, A. Carrington, P. Fournier, R. L. Greene, P. Guptasarma, D. G. Hinks, and A. R. Banks, *Appl. Phys. Lett.* **77**, 4202 (2000).
- [39] R. J. Ormeno, A. Sibley, C. E. Gough, S. Sebastian, and I. R. Fisher, *Phys. Rev. Lett.* **88**, 047005 (2002).
- [40] H. Kim, M. A. Tanatar, R. Flint, C. Petrovic, R. Hu, B. D. White, I. K. Lum, M. B. Maple, and R. Prozorov, *Phys. Rev. Lett.* **114**, 027003 (2015).
- [41] H. Kim, N. H. Sung, B. K. Cho, M. A. Tanatar, and R. Prozorov, *Phys. Rev. B* **87**, 094515 (2013).
- [42] M. A. Tanatar, J. Paglione, C. Petrovic, and L. Taillefer, *Science* **316**, 1320 (2007).
- [43] D. Saint-James and P. Gennes, *Phys. Lett.* **7**, 306 (1963).
- [44] H. Baek, J. Ha, D. Zhang, B. Natarajan, J. P. Winterstein, R. Sharma, R. Hu, K. Wang, S. Ziemak, J. Paglione, Y. Kuk, N. B. Zhitenev, and J. A. Stroscio, *Phys. Rev. B* **92**, 094510 (2015).
- [45] A. Banerjee, A. Fang, C. Adamo, P. Wu, E. Levenson-Falk, A. Kapitulnik, S. Chandra, B. Yan, and C. Felser, *APS Meeting Abstracts* (2005), Vol. 1, p. 25005, <http://meetings.aps.org/link/BAPS.2015.MAR.T25.5>.
- [46] Q.-Z. Wang, J. Yu, and C.-X. Liu, *Phys. Rev. B* **97**, 224507 (2018).
- [47] R. Prozorov, D. D. Lawrie, I. Hetel, P. Fournier, and R. W. Giannetta, *Phys. Rev. Lett.* **93**, 147001 (2004).
- [48] R. Prozorov, M. D. Vannette, R. T. Gordon, C. Martin, S. L. Bud'ko, and P. C. Canfield, *Supercond. Sci. Technol.* **22**, 034008 (2009).
- [49] P. Prommapan, M. A. Tanatar, B. Lee, S. Khim, K. H. Kim, and R. Prozorov, *Phys. Rev. B* **84**, 060509(R) (2011).
- [50] H. Kim, M. A. Tanatar, Y. J. Song, Y. S. Kwon, and R. Prozorov, *Phys. Rev. B* **83**, 100502(R) (2011).
- [51] N. H. Sung, Y. J. Jo, and B. K. Cho, *J. Appl. Phys.* **109**, 07E109 (2011).
- [52] L. Savary, J. Ruhman, J. W. F. Venderbos, L. Fu, and P. A. Lee, *Phys. Rev. B* **96**, 214514 (2017).
- [53] J. Ruhman and P. A. Lee, *Phys. Rev. B* **94**, 224515 (2016).
- [54] L. P. Gor'kov, *Proc. Natl. Acad. Sci. USA* **113**, 4646 (2016).
- [55] I. Boettcher and I. F. Herbut, *Phys. Rev. Lett.* **120**, 057002 (2018).
- [56] G. B. Sim, A. Mishra, M. J. Park, Y. B. Kim, G. Y. Cho, and S. B. Lee, *Phys. Rev. B* **100**, 064509 (2019).
- [57] J. W. F. Venderbos, L. Savary, J. Ruhman, P. A. Lee, and L. Fu, *Phys. Rev. X* **8**, 011029 (2018).
- [58] B. Roy, Sayed Ali Akbar Ghorashi, M. S. Foster, and A. H. Nevidomskyy, *Phys. Rev. B* **99**, 054505 (2019).
- [59] W. Yang, T. Xiang, and C. Wu, *Phys. Rev. B* **96**, 144514 (2017).
- [60] R. T. Gordon, N. D. Zhigadlo, S. Weyeneth, S. Katrych, and R. Prozorov, *Phys. Rev. B* **87**, 094520 (2013).